Investigating the Aerodynamic Impacts of Laser-Based Ablation on a Carbon Fiber Composite in a Mach 3.5 Shock/Boundary-Layer Interaction

Seth Pickman* and Jalen Johnson†
University of Tennessee, Knoxville, TN, 37996, United States of America

Phillip Kreth‡
University of Tennessee Space Institute, Tullahoma, TN, 37388, United States of America

This study investigates the aerothermodynamic impacts of localized material ablation on a Mach 3.5 shock-wave/boundary-layer interaction (SBLI). To study these types of effects in a low-enthalpy ground test facility such as those typically available in a university lab setting, a 500 W continuous-wave (CW) laser was ported into the Mach 3.5 blowdown wind tunnel to induce active, *in-situ* ablation. A cone-slice-ramp model was equipped with a flush-mounted carbon-fiber composite test coupon ahead of the ramp that generates the SBLI. Flow field disturbances and surface temperature gradients were evaluated using high-speed schlieren imaging and Temperature-Sensitive Paint (TSP). Analysis of the schlieren images revealed that the active ablation of the carbon fiber composite matrix increases the angle of the ramp-generated oblique shock, though the separation shock is severely diminished. Furthermore, surface recession and cratering permanently altered the post-ablation aerodynamic footprint of the test coupons. TSP measurements over the ramp (downstream of the test coupon) confirmed intense localized heat transfer occurs during the laser irradiation; however, the accumulation of ablation debris on the ramp surface impacts the TSP-based temperature readings through optical interference (which appears to inflate the temperature), highlighting unique diagnostic challenges in tests where ablation occurs.

Nomenclature

I	=	Intensity, W/m^2
I_{ref}	=	Intensity of Reference Image, W/m^2
M	=	Freestream Mach number
P_0	=	Stagnation pressure, kPa
Re_x	=	Unit Reynolds Number, m^{-1}
SBLI	=	Shock-Wave/Boundary-Layer Interaction
T	=	Temperature, K
T_0	=	Stagnation temperature, K
T_{ref}	=	Reference Temperature, K
TSP	=	Temperature-Sensitive Paint
UTSI	=	University of Tennessee Space Institute
λ	=	Laser wavelength, nm

I. Introduction

THERMAL protection system materials deployed on the leading edges and control surfaces of hypersonic vehicles are subjected to extreme aerodynamic heating, aggressive chemical reactions, and surface erosion [1]. These coupled

*Undergraduate Research Assistant, University of Tennessee, AIAA Student Member.
†Undergraduate Research Assistant, University of Tennessee, AIAA Student Member.
‡Associate Professor, Mechanical and Aerospace Engineering, and AIAA Associate Fellow.

aerothermodynamic phenomena threaten vehicle performance and structural survivability. Despite decades of research, the transient response of ablative materials under realistic hypersonic flow conditions remains poorly characterized in the public domain [2]. This knowledge gap is largely driven by the fundamental limitations of current ground-test facilities. Shock tubes provide the necessary high enthalpy but suffer from extremely short test times that cannot capture sustained ablation [3]. Conversely, conventional blowdown wind tunnels offer longer run times, but they typically lack the total enthalpy required to initiate and sustain material degradation [4]. While arc-heated facilities can maintain the appropriate high-enthalpy conditions for extended durations, they are incredibly expensive to build, maintain, and operate, and they are not widely accessible with immense schedule pressure due to their rarity. Moreover, the flow quality in arc-heated facilities can be problematic towards developing an understanding of true material responses [5, 6].

Laser irradiation and ablation of material test coupons integrated into wind tunnel models offers a potential robust solution to some limitations associated with ground testing. High-powered continuous-wave (CW) lasers can produce controllable localized surface heating loads, emulating the effects of high-enthalpies near these regions, without the need to heat the entire freestream flow. When integrated into an optically accessible supersonic wind tunnel, an external high-power laser allows for the systematic investigation of material response, ablation plume dynamics, and flow-material interactions under highly repeatable aerodynamic conditions. This architecture also provides modularity, allowing researchers to switch or move laser sources or alter heating/ablation profiles (e.g., by controlling the laser power, exposure duration) without modifying the primary wind tunnel infrastructure.

Understanding the aerodynamic impact of ablation is particularly critical in regions where shock-wave/boundary-layer interactions (SBLIs) occur as both of these phenomena can be unsteady, and potentially coupled. In supersonic flight, separating and reattaching shear layers significantly amplify local heat transfer and pressure loads. For example, fins or pylons can experience extreme heating as a result of potential shock-shock interactions (SSIs) that arise from their SBLIs, with perhaps the most notable example of this being the loss of the dummy ramjet model off of the X-15A-2 [7]. When an ablating surface interacts with an SBLI, the resulting outgassing, surface recession, and time-varying roughness will likely alter the size and unsteadiness of the boundary layer. To investigate these highly coupled effects, this research details the application of *in-situ*, laser-based augmented heating and ablation using a 500 W continuous-wave, infrared (IR) laser ported into the recently-upgraded Mach 3.5 blowdown wind tunnel at the University of Tennessee Space Institute (UTSI). In these experiments, a cone-slice-ramp model was used to integrate flat carbon fiber composite test coupons ahead of the ramp (i.e., on the slice). By placing the test coupons in front of the ramp, the SBLI generated by the compression ramp will be impacted by the laser irradiation. In this paper, we summarize the experiments conducted with high-speed schlieren imaging and temperature-sensitive paint (TSP), with and without laser heating, to characterize the effects of localized heating and ablation on the SBLI.

II. Experimental Facility and Laser Integration

A. UTSI's Mach 3.5 Blowdown Wind Tunnel

All experimental data were collected in the Mach 3.5 blowdown wind tunnel at UTSI. The facility expands high-pressure air to Mach 3.5 conditions across an 8" x 8" test section with the stilling chamber pressure maintained by a pressure-regulating valve during each run. The air supplied to the tunnel is unheated, but its dewpoint is sufficiently low to prevent condensation during runs which are typically kept to approximately 5-10 seconds. The steady-state flow over this duration is sufficient for establishing steady aerodynamic conditions with controlled stagnation pressures. The wind tunnel was recently upgraded from a Mach 2 configuration, and heavy emphasis was placed on optical access for non-intrusive flow diagnostic techniques such as high-speed schlieren imaging and particle image velocimetry (PIV). Recent facility characterization efforts indicate that freestream turbulence levels are approximately 1.1% in the rear test section, where the model was located, based on post-shock pitot pressure fluctuations (i.e., rms of $P'_{0,2}$). The boundary layer thickness on the ceiling and floor of the test section were measured to be approximately 0.69" in thickness based on the local flow reaching 99% of the freestream velocity which was measured to be 622 m/s at a stilling chamber pressure and temperature of $P_0 \approx 120$ psia and $T_0 \approx 285$ K, respectively. At these conditions, the Mach 3.5 wind tunnel produces flow in the test section with a unit Reynolds number of $Re_x \approx 51.5$ million m^{-1} (15.7 million ft^{-1}).

B. High-Power Laser System

Controlled surface heating and active material ablation are driven in these experiments by a fiber-coupled, continuous-wave diode laser (LaserLine LDM 500-60) operating at a wavelength between λ = 900–910 nm. While the nominal optical power output of the system is rated up to 500 W, *in-situ* power measurements indicated a maximum delivered power of P_{laser} = 415 W at the target surface (i.e., the carbon fiber composite test coupons on the slice portion of the cone-slice-ramp model). The laser focuses onto a square shape that measures approximately 11 mm x 11 mm about 200 mm away from the aperture on the laser head.

The optical fiber-coupled laser remains outside of the wind tunnel test section on an optical benchtop that sits underneath the tunnel. The IR laser beam is delivered through the high-power optical fiber to the laser head which was mounted above the test section. The laser passes through a small, flush-mounted sapphire window installed in the top wall of the wind tunnel. The laser power and shutter are controlled externally from the wind tunnel control room such that the material test coupons could be pre-heated prior to tunnel startup and ablated with varying laser power levels during the steady-state flow duration.

Two photographs of the area around the Mach 3.5 wind tunnel are shown in Fig. 1. Components of a Z-Type schlieren flow visualization system are visible along with the IR laser and the TSP diagnostic system. The cone-slice-ramp model are seen mounted in the test section in Fig. 1(a) where the flow direction is left-to-right. Further details about the diagnostic techniques used in these experiments are provided in the next section.

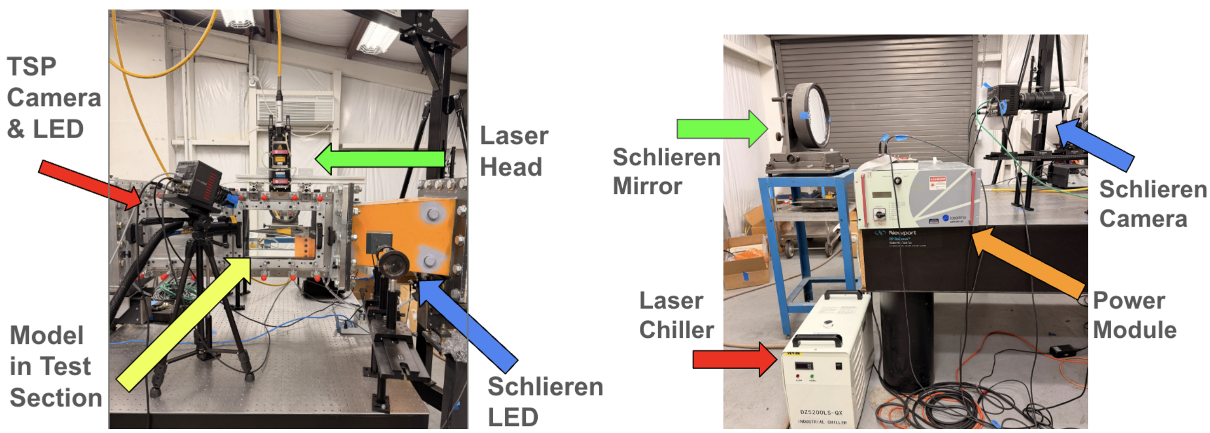

(a) Right Side of Test Section

(b) Setup to the Left of Test Section

Fig. 1 Experimental setup at the wind tunnel test section. (a) Schlieren illumination side of the tunnel with the laser head and TSP setup visible, and (b) schlieren collection side of the tunnel showing the laser chiller and power module.

C. Test Article Design: Cone-Slice-Ramp Model

Since the carbon fiber composite material of interest to the present study is commercially-available in flat sheet formats only, individual test coupons of the material samples could only be integrated into flat sections of a wind tunnel model. To best facilitate this with minimal unsteady starting loads and the lowest risk of unstarting the wind tunnel, a cone-slice-ramp geometry was selected for this study (as opposed to a larger flat plate model). The material test coupons, which were cut out of 1/8" thick carbon fiber composite sheets from DragonPlate® into squares measuring 1" by 1", could be easily integrated into the flat portion of the cone-slice-ramp model (i.e., where the slice was made). The downstream compression ramp at the aft end of the model generates an SBLI that will be affected by the laser irradiation creating augmented heating or ablating the material test coupons.

The cone-slice-ramp geometry is a canonical configuration that has been frequently utilized to study complex flow separation, shear layer instability, and SBLI behavior in high-speed flow regimes [8, 9]. The model used in the present study is similar to others in that it features a 7-degree half-angle cone that then transitions into a flat slice which has a 20-degree compression ramp at the aft end. The base cone geometry is a standard geometry for fundamental aerodynamic characterization [10], and others have used similar cone-slice-ramp configurations [11–13]. This model was machined from SAE 304 stainless steel due to its strength and thermal resistance/durability.

To facilitate rapid, repeated testing of various material samples, the model was designed with a recessed insert on the sliced portion to accommodate interchangeable material test coupons. The 1/8" thick DragonPlate® inserts were used for all experimental runs including the unheated baseline aerodynamic characterizations. These inserts are secured

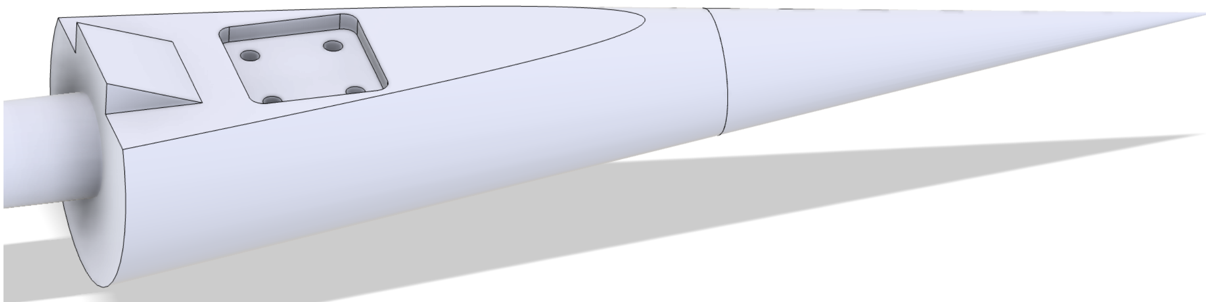

Fig. 2 Perspective view of the CAD model of the 7-degree half-angle cone-slice-ramp model geometry used in the present study. The compression ramp angle is 20 degrees.

flush with the model surface using four (steel) countersunk screws. To protect the underlying stainless-steel model structure from the intense localized heating, an 1/8" thick piece of ceramic fiber furnace blanket is installed directly beneath the test coupons to serve as an insulation layer. Additionally, a fast-response, K-type thermocouple is embedded in the model between the DragonPlate® test coupons and the ceramic insulation to monitor the internal temperature response during varying laser irradiation and sustained exposure to the aerodynamic flow field.

III. Diagnostic Methodologies

A. High-Speed Schlieren Imaging

High-speed schlieren imaging was used as the primary flow visualization tool for observing density gradients present within this flow field, such that shock structures, boundary-layer behavior, and SBLI dynamics could be seen. A modified Z-type configuration is used in this setup where a flat, first-surface mirror folds the light on the imaging side of the tunnel to help focus at the test section centerline. A vertical knife edge was used such that the horizontal density gradient are visualized within the schlieren images. Approximately half of the light was cut off at the knife edge as verified by measurements of the image intensities during adjustment of the knife edge. Images were collected with a Photron Mini UX-50 high-speed camera at frame rates between 1–10 kHz, depending on the desired temporal & spatial resolution of the specific experimental runs. Synchronized illumination was provided by a white LED (Luminus Devices CBT-140) pulsing at the same rates, with pulse widths set to 1 μs. The short duration illumination ensures that the high-speed flow over the model is effectively frozen in the instantaneous images. Qualitative assessments of the schlieren images revealed that measurable impacts were observed when the laser was active in either preheating or ablating the material test coupons. Quantitative evaluation of these images were used to determine the differences in the structure of the flow field (e.g., shock wave angles, extent of shock wave dynamics).

B. Temperature-Sensitive Paint (TSP)

Temperature-sensitive paint (TSP) provides a non-intrusive method for directly visualizing surface temperature changes on a model that is exposed to an aerothermodynamic environment. In this set of experiments, the TSP formulation was applied to removable adhesive-backed sheets that were securely attached to the surface of the 20-degree compression ramp. Prior work at UTSI conducted by Edwards, et al. [14] demonstrates the viability of using adhesive-backed Temperature-Sensitive Paint (TSP) films for quantitative aerodynamic heating measurements. In their study, a hot plate uniformly heated steel plates that were coated with various TSP and polyvinyl chloride (PVC) film configurations. Reaching temperatures up to approximately 383 K, they observed a consistent quadratic relationship between the temperature ratio (T/T_{ref}) and the luminescence intensity ratio (I/I_{ref}). They concluded that applying the TSP top coat directly to a PVC film prepared with light surface sanding yielded calibration curve coefficients with minimal deviation from traditional paint applications, validating the adhesive film approach used in the present study.

Illumination of the paint is provided by a UV LED from Innovative Scientific Solutions, Inc. (ISSI). The UV LED is turned on before the data collection period to ensure it reaches a steady-state output. Emission from the paint is proportional to the surface temperature (details on this are provided below), and this is monitored by a Photron Mini AX-200 high-speed camera. The UV excitation and IR laser irradiation are blocked by optical filters placed in front of the camera lens. An additional bandpass optical filter is used to prevent excess light collection from the material sample as it heats up to temperatures, causing visible light emission.

The TSP calibration was conducted *in-situ* using an additional painted sample that was installed on top of the carbon fiber composite test coupon. A separate K-type thermocouple was placed beneath the TSP sample to determine the local temperature. The IR laser was used as a highly controllable heat source for the TSP sample. By operating the laser at low power settings with fine incremental adjustments, the TSP calibration sample was allowed to reach a steady-state temperature at each calibration point. Once thermal equilibrium was established at a given setpoint, the high-speed camera recorded 1,001 images of the TSP sample. These images were averaged both temporally and spatially over the painted region of interest in a post-processing routine to extract a single mean paint emission intensity for each temperature condition, considered the wind-off reference condition. This procedure was repeated across six distinct temperature setpoints ranging from 21.6°C to 99.1°C.

The initial unheated baseline state, which was recorded at 21.6°C, serves as the reference condition for both temperature (T_{ref}) and intensity (I_{ref}). The subsequent intensity ratios (I/I_{ref}) and temperature ratios (T/T_{ref}) are fitted with a second-order polynomial, yielding the following relationship:

$$\frac{T}{T_{\mathrm{ref}}} = 0.3441\left(\frac{I}{I_{\mathrm{ref}}}\right)^2 - 0.6594\left(\frac{I}{I_{\mathrm{ref}}}\right) + 1.3223 \quad (1)$$

This specific quadratic calibration curve is used to convert the TSP image intensities into quantitative surface temperature maps. Before each tunnel run, an additional 1,001 images were recorded (without the flow), and the resulting average image is used as I_{ref} for the following run. The temperature of the air inside the tunnel was measured by the tunnel control program during this period, and this value is used as T_{ref} for that run.

A final noteworthy observation about the TSP measurements is that the painted region inadvertently served an additional diagnostic purpose in that the ablation products impacted and accumulated on the surface of the paint. The distinct patterns that were observed after the flow and laser exposures provided a direct, physical visualization of the SBLI flow topology, highlighting regions on the compression ramp where heating and ablation impacts were most significant. Although not discussed in this paper, these observations are being explored.

IV. Results & Discussion: High-Speed Schlieren Imaging

High-speed schlieren imaging captures the dynamic density gradients, shock structures, and ablation plume interactions within the Mach 3.5 flowfield. To fully isolate the aerodynamic impacts of the laser-induced ablation, the flow topology was evaluated across three distinct experimental phases: the baseline case with undamaged material test coupons, the active laser-heating / ablation phase, and the post-exposure state.

A. Nominal Baseline Flow Topology

Prior to laser irradiation, a baseline wind tunnel run was conducted over one of several pristine 1/8"thick DragonPlate® carbon-fiber inserts / test coupons. A handful of test coupons were cut from a larger sheet, and each coupon is easily interchangeable. The schlieren imaging from this run establishes the reference flow field of the shock-wave/boundary-layer interaction (SBLI) generated by the 20-degree compression ramp. In this baseline flow state, the incoming boundary layer separates ahead of the ramp corner, forming a distinct separation shock which is visible in Fig. 3a. Here, approximately 5,000 images have been averaged together to showcase the mean flow structure over the model. The current view showcases the entirety of the slice and ramp, though the cone's leading edge tip extends outside of this field of view. The fore and aft ends of the test coupon are not perfectly flush with the surrounding metal of the model; therefore, weak shocks are observed at these interface locations. Downstream, at the compression ramp, the typical SBLI structure for such a configuration is observed. A separation bubble extends slightly upstream from the ramp's leading edge, creating a separation shock which forms the forward shock foot of the lambda-shock structure. It is difficult to distinguish between the reattachment shock and the inviscid oblique shock that both emanate from such an interaction; however, the coalescing shocks do serve as a distinct characteristic in the images. Additional waves are seen in the flow over the test coupon as its surface is rough in comparison with the surrounding metal.

B. Modified Flow State with Active Heating & Ablation

Following the wind tunnel runs that established the baseline flow topology, the 415 W continuous-wave laser was focused onto the test coupon while the Mach 3.5 freestream flow was established. During these tests, the intense laser irradiation was focused onto an 11 mm x 11 mm square centered on the carbon-fiber coupon. Upon localized heating, the carbon-fiber matrix rapidly outgases and ablates. Traces of the ablation plume can be seen in the averaged schlieren image in Fig. 3b, and close inspection of the boundary layer and SBLI regions reveals that they have been impacted by the intense laser heating of the test coupon. The high-temperature region over the test coupon increases the boundary layer thickness, thereby modifying the SBLI downstream.

Although the laser-based heating is localized, the impacts are observed downstream as the heated air and ablation products convect downstream. The schlieren images show that the separation shock is noticeably displaced relative to the baseline condition. This comparison is best observed in Fig. 3c where the difference was taken between laser exposure case and the baseline case (i.e., Fig. 3c = Fig. 3b - Fig. 3a). Here, positive and negative deviations are shown on the diverging red/blue colormap, where a positive deviation indicates that the schlieren image with the laser exposure has a brighter intensity at that region.

The laser heating increases the angle of the oblique shock generated by the ramp, as can be seen from the dark blue line in Fig. 3c, although this effect is more clearly observed by flipping between the images. At the base of the shock interaction, a distinct red region indicates that the original separation shock was modified as well. Inspection of the time-averaged schlieren image with the laser exposure (Fig. 3b) shows that the separation shock has seemingly dissipated. Many of the weaker waves from above the test coupon in the baseline case have also vanished.

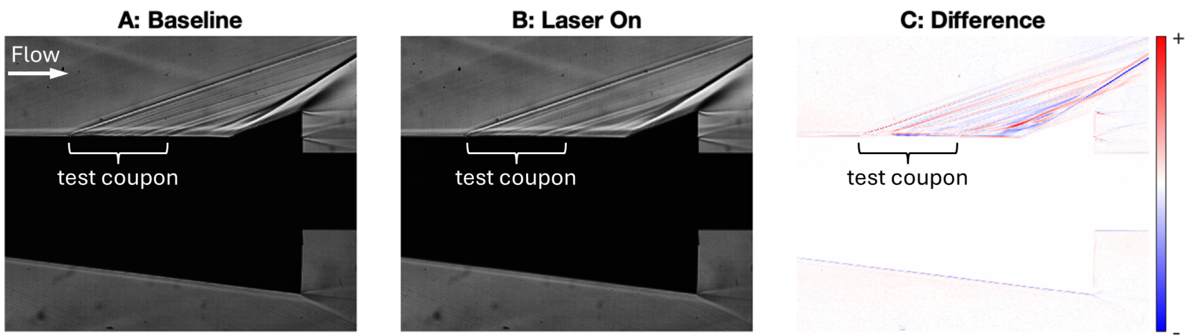

Fig. 3 Time-averaged schlieren images for (a) the baseline case and (b) the case with active laser exposure on the test coupon. The third image in (c) is the difference between these two cases (Laser - Baseline).

C. Post-Ablation Aerodynamic Effects

Following the tests with the active laser-based heating / ablation of the test coupon, a repeat tunnel run was conducted without the laser heating to investigate the effects of the laser-induced damage on the flow field. Inspection of the model after the laser exposure revealed that permanent morphological changes did occur, confirming that substantial ablation took place during the laser exposure run. The laser irradiation resulted in localized surface recession, matrix depletion, and increased surface roughness on the composite insert. Averaging the schlieren images from this post-ablation run reveals that the local flow field and the SBLI do not match the baseline state (when the test coupon was undamaged). The roughened topology of the ablated region modifies the local flow flowfield over the test coupon as can be seen in Fig. 4b. Comparing the flow over the damaged coupon with that of the original baseline state (Fig. 4a), the impact of the degraded surface is clear: additional waves are present as a result of the recessed material and the roughness of the exposed matrix. These effects are more readily apparent in the difference image which is shown in Fig. 4c. As before, the intensities from the baseline state are subtracted from those with the damaged coupon. A slight shift in the inviscid oblique shock produced by the ramp can be seen, but the most substantial impacts are localized in the region above the damaged test coupon. It appears as though there were little impacts on the lambda shock foot structure as the separation shock seems to be in the same location. The laser exposure was limited to approximately 10 seconds, so perhaps a longer exposure would have yielded more substantial impacts that would have affected the SBLI more significantly.

Photographs of a typical 1" x 1" x 1/8"-thick DragonPlate® material test coupon used in these experiments are shown in Fig. 5. The undamaged carbon fiber coupon (Fig. 5a) is attached to the slice on the cone-slice-ramp surface

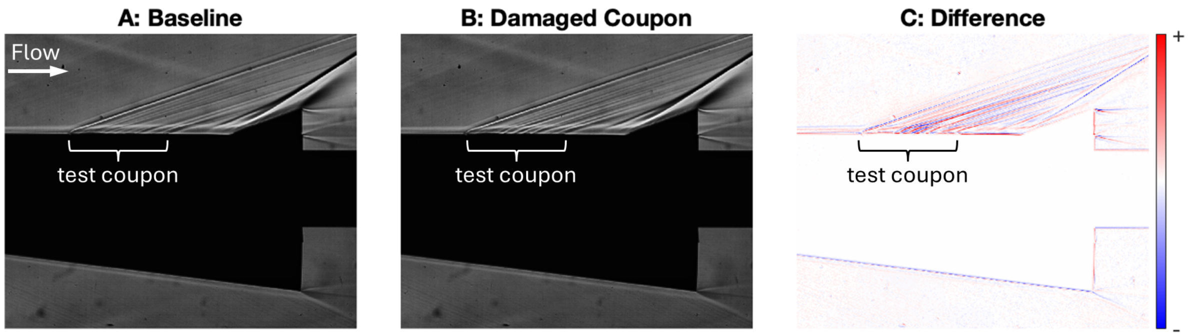

Fig. 4 Time-averaged schlieren images for (a) the baseline case [repeated here] and (b) the post-exposure case with the damaged test coupon. The third image in (c) is the difference between these two cases (Damaged - Baseline).

with four countersunk screws. The IR laser was focused to an 11 mm x 11 mm square at the center of the test coupon as can be seen from the damage shown in Fig. 5b. Ablation and outgassing of the material has occurred, exposing the underlying carbon fiber matrix as pictured. From these photographs, it is clear how the damaged coupon causes the local flow field to have additional distortions present as seen in the time-averaged schlieren images.

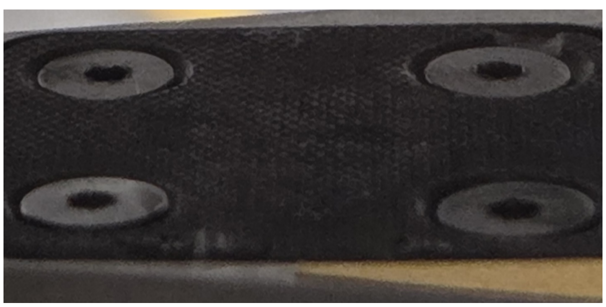

(a) Undamaged carbon fiber composite test coupon installed in the model

(b) The same material test coupon after laser and flow exposure showing the damaged surface

Fig. 5 Photographs comparing a material test coupon before and after it was exposed to laser irradiation and Mach 3.5 flow.

V. Results & Discussion: Temperature-Sensitive Paint (TSP) and Back-Temperatures

Because of how the laser is ported into the wind tunnel test section, the TSP camera is unable to have a direct line of sight that is perfectly orthogonal to the ramp or model surface. The larger field of view from this high-speed camera was cropped to a rectangular region of interest (ROI) that encompasses the painted surface on the 20-degree compression ramp. This can be seen in Fig. 6 which shows the full field of view and demonstrates the region of interest for the TSP data processing. Photogrammetry techniques were not used to transform this viewing area into streamwise and spanwise coordinates; instead, the mapping of these images is conducted with the displayed perspective and ROI. Consequently, the freestream flow direction traverses the bottom-left to the top-right of the images.

The raw TSP images were processed by time-averaging the wind-on frames of each recording and dividing by the time-averaged wind-off reference frame. These intensity ratios were then converted to temperatures with the calibration curve found earlier. The temperature measured during the acquisition of the reference images was used for T_{ref} in the conversion from intensity ratios. To mitigate pixel-level noise and improve the clarity of the data, a spatial smoothing

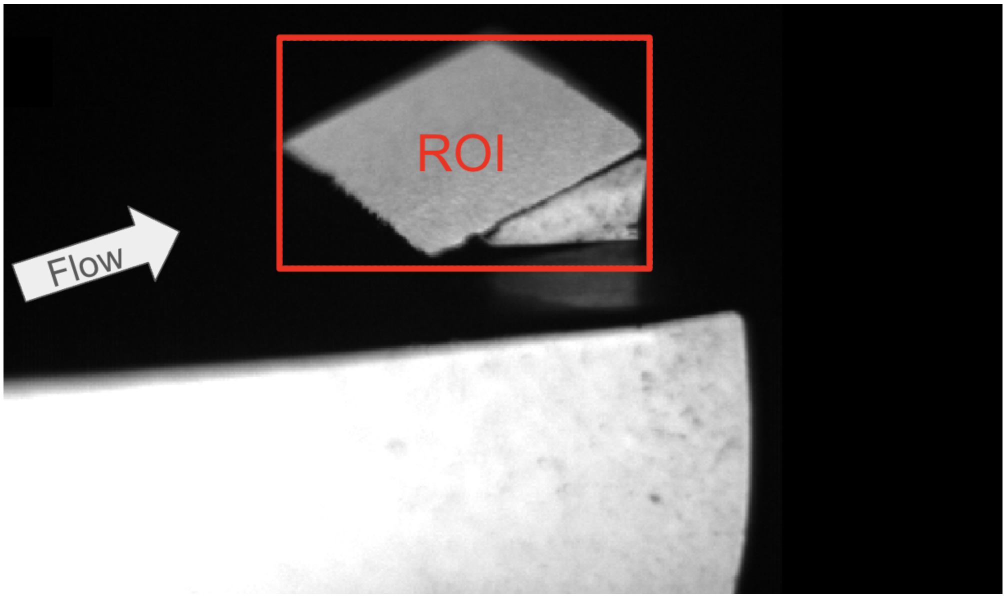

Fig. 6 A typical instantaneous image showing the TSP camera field of view and the defined region of interest (ROI) used in processing the surface temperatures over the ramp.

algorithm was applied to the resulting temperature maps. The adhesive TSP films were changed at the same time as the material test coupons. In this manner, a single TSP film was paired with a particular carbon fiber test coupon for a series of wind tunnel runs. During the tunnel run with active laser irradiation, ablated material and soot impacted the TSP film, altering the TSP surface through the material deposition and/or damaging the TSP paint. Accumulation of ablated material on the TSP film required that the wind-off reference frames could correct for the reduced fluorescence emission from those portions of the coupons; however, these effects could not be mitigated. As a result, there are high uncertainties in the measured TSP temperatures for the cases of both active laser irradiation and the damaged coupon. It is important to note that the three cases (baseline, laser exposure, and damaged coupon) were tested in separate wind tunnel runs. Results showing the temperature maps over the compression ramp for these cases can be seen in Fig. 7.

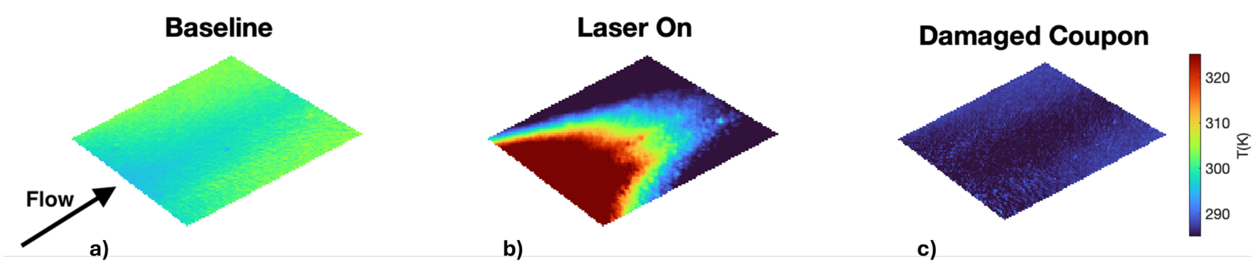

Fig. 7 Time-averaged TSP results showing the impact of localized laser heating / ablation. Left: baseline flow. Middle: flow with the laser actively irradiating the test coupon upstream. Right: flow without laser heating using the damaged test coupon.

Figure 7a shows the baseline surface temperature distribution across the compression ramp exposed to the unheated Mach 3.5 flow conditions. The temperature across the ramp is uniform, with only slight variations occurring in the spanwise direction. The baseline temperature levels are approximately 300 K. During the subsequent test with active laser heating (the case shown in Fig. 7b), a distinct increase in the surface temperature is observed at the base of the ramp. This is certainly to be expected as the material test coupon is located a short distance upstream of the ramp, and the laser irradiation is drastically increasing the local surface temperature of the coupon. Additionally, the coupon did undergo ablation during this run, so some of the elevated temperatures may be erroneously displayed as damage to the TSP film or the accumulation of ablation products will result in a loss of emission which corresponds to a higher temperature through the conversion from intensities. Inspection of the model after this run did show that some of the TSP film in this area was impacted by material accumulation and potentially damage caused by the impact of these ablation products on the film itself. These results were consistent across additional experiments with active laser heating that were conducted but are not shown in this paper.

The final wind tunnel run for this particular carbon fiber coupon was conducted after the laser ablation test and subsequent model inspection. The results from this post-ablation run show how the temperature distribution across the ramp is affected by the laser-damaged carbon fiber test coupon. Figure 7c shows the TSP results for this case. As with the baseline case, there is a uniform surface temperature distribution across the ramp, save for some minute variations in the spanwise direction. In contrast to the original baseline case, the temperatures observed on the ramp downstream of the damaged coupon are lower, with an average surface temperature being approximately 290 K. Upon reviewing these data, we believe that the rapid testing pace between these cases likely caused these surface temperatures to be lower than expected. For blowdown wind tunnels without heated air supplies, a faster testing pace can result in colder temperatures being experienced in the flow due to the expansion of air from the high-pressure supply tanks.

While no direct temperature measurement was acquired with a transducer placed on/within the ramp, a K-type thermocouple was placed between the material test coupon and the insulation material mounted underneath it. Data were acquired from this thermocouple at a rate of 100 Hz, and over a duration that fully encompassed the wind tunnel run and a few seconds prior to and after the flow. Figure 8 presents the coupon back-temperature histories throughout each of the aforementioned test cases. These time histories have been aligned at the point in time where the tunnel flow was initiated (i.e., time $t = 0$ s). The vertical dashed lines overlaying the time histories indicate when the tunnel was shut down for each of the runs. It is clear that the case with laser heating has a substantial rise in the coupon back-temperature over the duration of the laser exposure and even for a couple of seconds after the flow has been shut off. Comparisons of these temperature data can be made with those from a partner study in which the ablation of similar material test coupons was studied in an evacuated test chamber, although these comparisons are outside the scope of the present paper.

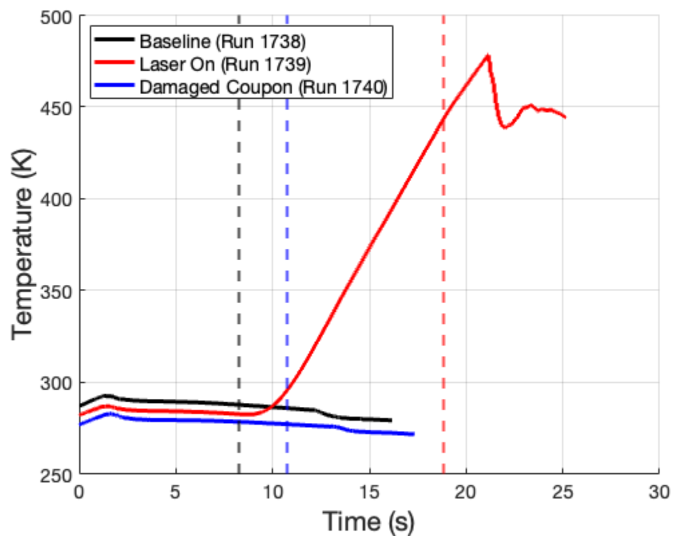

Fig. 8 Time histories of the material test coupon back-temperature during the runs discussed in this paper.

VI. Conclusions and Proposed Future Work

An experimental investigation was conducted to characterize the aerodynamic and thermal effects of laser-based heating and ablation on carbon fiber composite test coupons placed on a cone-slice-ramp model subjected to a Mach 3.5 freestream flow. The material test coupons were located upstream of the ramp on the slice portion of the model such that the laser irradiation effects could be observed on the ramp-generated SBLI. A 500 W continuous-wave laser was ported into the test section of UTSI's Mach 3.5 blowdown wind tunnel to irradiate these material samples prior to and during the flow exposure. By controlling the laser power externally, localized heating and ablation was achieved without the need to heat the entire freestream flow in the tunnel to sufficient total enthalpies that would cause ablation.

High-speed schlieren imaging demonstrated that active ablation significantly disrupts the local flow topology. The high-temperature outgassing of the carbon fiber composite material increased the boundary layer thickness and introduced disturbances that seemed to mitigate the separation within the SBLI. Assessment of the material coupon after the flow and laser exposure revealed that permanent morphological changes occurred in the composite. Cratering, loss of mass & material, and increased roughness through the exposure of the carbon fiber matrix altered the boundary layer, preventing the SBLI from fully returning to its baseline state.

Surface temperature distributions were measured over the ramp by applying temperature-sensitive paint (TSP) to adhesive-backed films that were then attached to the ramp. The TSP measurements captured distinct heating footprints during laser irradiation. However, the results underscored a critical diagnostic limitation: the deposition of upstream ablation products onto the TSP film significantly interfered with its emission, thereby artificially inflating perceived temperatures.

Future research efforts in this area should aim to address this limitation by incrementing the laser power up to the point that ablation occurs. Additionally, in this effort, the time between subsequent tunnel runs was limited, and this impacted the model and flow temperatures prior to and during the runs. A slower pace of testing would have allowed for these temperatures to relax to the same initial state for better comparisons between the cases before and after the laser exposure. Ultimately, this research validates the utility of localized laser-based heating for studying ablative material responses in conventional (i.e., low enthalpy) supersonic facilities.

VII. Acknowledgements

Funding for this research effort was provided by the U.S. Navy under award number N001782510015 entitled Hypersonic-focused Engineering Research and Outreach for Undergraduate Training (HERO-UT). The authors would also like to acknowledge John Strike for his extensive engineering support throughout this project, Dr. Cary Smith for lending his expertise in setting up and processing data from the temperature-sensitive paint diagnostic, and the UTSI machine shop staff for their diligence in fabricating the model used in this study.

References

[1] Uyanna, O., and Najafi, H., "Thermal protection systems for space vehicles: A review on technology development, current challenges and future prospects," *Acta Astronautica*, Vol. 176, 2020, pp. 341–356. https://doi.org/https://doi.org/10.1016/j.actaastro.2020.06.047, URL https://www.sciencedirect.com/science/article/pii/S0094576520304148.

[2] Wang, H., et al., "Oxidation and Sublimation Ablation of C/SiC Ceramics in Hypersonic Environments," *AIAA Journal*, 2025. https://doi.org/10.2514/1.A36501.

[3] Zander, F., Morgan, R. G., Sheikh, U. A., Buttsworth, D. R., and Teakle, P. R., "Hot-Wall Reentry Testing in Hypersonic Impulse Facilities," *AIAA Journal*, Vol. 51, No. 2, 2013, pp. 476–484. https://doi.org/10.2514/1.J051867.

[4] Gu, S., and Olivier, H., "Capabilities and limitations of existing hypersonic facilities," *Progress in Aerospace Sciences*, Vol. 113, 2020, p. 100607. https://doi.org/10.1016/j.paerosci.2020.100607.

[5] Cipullo, A., Noack, B. R. R. R., and Chazot, O., "Investigation of a Free-Stream Air Plasma Flow by Optical Emission Spectroscopy and Comparison to Magnetohydrodynamics Simulations," *AIAA SciTech 2020 Forum*, American Institute of Aeronautics and Astronautics, Orlando, Florida, 2020. https://doi.org/10.2514/6.2020-0382.

[6] O'Brien, A. C., Ivey, C. B., et al., "Particle Image Velocimetry and Total Temperature Characterization of Arc-Heated Mach 4.5 Free Jet," *AIAA Journal*, Vol. 62, No. 4, 2024, pp. 1485–1498. https://doi.org/10.2514/1.J063531.

[7] Dana, W., "The X-15 airplane—Lessons learned," *31st Aerospace Sciences Meeting*, American Institute of Aeronautics and Astronautics, Reno, NV, 1993. https://doi.org/10.2514/6.1993-309, URL https://arc.aiaa.org/doi/10.2514/6.1993-309.

[8] McKiernan, G., and Schneider, S. P., "Instability and Transition on a Cone with a Slice and Ramp at Mach 6," *AIAA SciTech 2021 Forum*, American Institute of Aeronautics and Astronautics, 2021. https://doi.org/10.2514/6.2021-0249.

[9] Francis, A. A., and Jewell, J. S., "Effect of Angle of Attack on Separation Bubble Instability and Transition on a Cone-Slice-Ramp in Mach-6 Quiet Flow," *AIAA SCITECH 2024 Forum*, American Institute of Aeronautics and Astronautics, 2024. https://doi.org/10.2514/6.2024-1104.

[10] Hyslop, A. M., McGilvray, M., and Doherty, L. J., "Free-Flight Aerodynamic Testing of a 7 Degree Half-Angle Cone," *AIAA SCITECH 2022 Forum*, American Institute of Aeronautics and Astronautics, 2022. https://doi.org/10.2514/6.2022-1324.

[11] McKiernan, G., and Schneider, S. P., "Instability and Transition on a Cone with a Slice and Ramp at Mach 6," *AIAA Scitech 2021 Forum*, American Institute of Aeronautics and Astronautics, 2021. https://doi.org/10.2514/6.2021-0249.

[12] Casper, K. M., Beresh, S. J., Spillers, R. W., et al., "Hypersonic Fluid–Structure Interaction on a Cone–Slice–Ramp Geometry," *AIAA Journal*, 2023. https://doi.org/10.2514/1.J062733.

[13] Rubio, J. S., Daniel, K., Swain, W., Downing, C. R., Lyon, B. T., and Wagner, J. L., "Investigating the Shock Wave-Boundary Layer Interaction in High-Enthalpy Hypersonic Flow Over a Cone-Slice-Ramp Geometry," *AIAA SciTech Forum*, American Institute of Aeronautics and Astronautics, 2026. https://doi.org/10.2514/6.2026-0871.

[14] Edwards, S., Constantin, R., Smith, C. D., and Gragston, M., "Development and Characterization of Adhesive Temperature Sensitive Paint Films for Aerodynamic Heating Measurements," *AIAA AVIATION FORUM AND ASCEND 2024*, American Institute of Aeronautics and Astronautics, Las Vegas, Nevada, 2024. https://doi.org/10.2514/6.2024-4275, URL https://arc.aiaa.org/doi/10.2514/6.2024-4275.